ARTICLE

Growth Mechanism of Vertically Aligned Carbon Nanotube Arrays

Ji-cheng Zhang[a], Yong-jian Tang[a], Yong Yi[b], Min-jie Zhou[a], Kang-fu Ma[a], Wei-dong Wu[a], Chao-yang Wang[a], Yan Zhao[a], Bing-chi Luo[a], Zhuo Wang[a]*

a. Science and Technology on Plasma Physics Laboratory, Research Center of Laser Fusion, China Academy of Engineering Physics, Mianyang 621900, China
b. College of Material Science and Engineering, Southwest University of Science and Technology, Mianyang 621010, China

(Dated: Received on February 9, 2015; Accepted on June 16, 2015)

Vertically aligned multi-walled carbon nanotube arrays grown on quartz substrate are obtained by co-pyrolysis of xylene and ferrocene at 850 °C in a tube furnace. Raman spectroscopy and high resolution transmission electron microscopy measurements show that the single-walled carbon nanotubes are only present on top of vertically aligned multi-walled carbon nanotube arrays. It has been revealed that isolated single-walled carbon nanotubes are only present in those floating catalyst generated materials. It thus suggests that the single-walled carbon nanotubes here are also generated by floating catalyst. Vertically aligned carbon nanotube arrays on the quartz substrate have shown good orientation and good graphitization. Meanwhile, to investigate the growth mechanism, two bi-layers carbon nanotube films with different thickness have been synthesized and analyzed by Raman spectroscopy. The results show that the two-layer vertically aligned carbon nanotube films grow "bottom-up". There are distinguished Raman scattering signals for the second layer itself, surface of the first layer, interface between the first and second layer, side wall and bottom surface. It indicates that the obtained carbon nanotubes follow the base-growth mechanism, and the single-walled carbon nanotubes grow from their base at the growth beginning when iron catalyst particles have small size. Those carbon nanotubes with few walls (typically <5 walls) have similar properties, which also agree with the base-growth mechanism.

Key words: Single-walled carbon nanotubes, Multi-walled carbon nanotubes, Growth mechanism, Microstructure characterization

I. INTRODUCTION

Vertically aligned carbon nanotube (CNT) arrays have attracted a lot of research interest since they were first synthesized in 1996 [1]. The vertically aligned CNT arrays with various structures have been obtained with interesting properties such as identical tube length, uniform orientation, and high purity. They can also be used as a field emission display, anisotropic conductive materials, multi-functional membranes, and super strong yarn [2−6]. These applications would become feasible if vertically aligned CNT arrays can be produced at a low cost on a large scale. The floating catalyst (FC) approach [7, 8] is a promising way because of its ability for continuous production of high-purity CNTs, its requirement of simple equipment, low reaction temperature, and low cost. Thus it has potential as an industrial process for high yield production of pure carbon nanotubes.

The growth mechanism of vertically aligned multi-walled carbon nanotube films on solid substrates has been reported [9, 10]. Only multi-walled carbon nanotube (MWCNT) existing in the vertically aligned CNT arrays products could be synthesized by the FC method [11, 12]. In this work, both single- and multi-walled carbon nanotubes (single-walled CNT on top of vertically aligned MWCNT arrays) have been synthesized in large quantities by the FC method. The so-obtained vertically aligned MWCNT array products were characterized by different approaches including high resolution transmission electron microscopy (HRTEM) and scanning electron microscopy (SEM), as well as Raman spectroscopy. MWCNTs were observed at high yield in a quartz tube reactor held at 850 °C. Single-walled carbon nanotubes (SWCNTs) were deposited with much lower yield at the tip of vertically aligned MWCNT arrays at the same time. HRTEM analyses revealed the only presence of isolated SWCNTs in the generated materials, although SWCNTs were typically observed in large bundles stabilized by van der Waals interaction between tubes [13]. Two-layer CNT films were synthesized at the same time. Through analyses of the char-

*Author to whom correspondence should be addressed. E-mail: wangzhuo@caep.cn, Tel.: +86-816-2480851, FAX: +86-816-2480830

acterization results obtained by HRTEM and Raman spectroscopy for the two-layers CNT films, the growth mechanism of MWCNT with SWCNT at the tip has been discussed in detail.

II. EXPERIMENTS

A. Synthesis

Vertically aligned MWCNT arrays were synthesized on a large scale by employing the FC method [14] in a horizontal tubular reactor made of quartz tube with a diameter of 60 and 400 mm in length. The reactor was inserted into a furnace that provided controllable heating up to 850 °C with a non-gradient temperature zone (reaction zone) of 150 mm in length. We measured the temperature distribution along the nanotube by K-type thermocouple. Xylene (C_8H_{10}) was used as the carbon source, ferrocene ($Fe(C_5H_5)_2$) as the catalyst precursor, and argon as the carrier gas. The optimization of the synthesis parameters was presented.

Xylene concentration was optimized by changing the flow rate of the carrier gas (argon) in the range of 1.0−1.5 L/min. Ferrocene concentration was optimized by changing the flow rate of the carrier gas, as well as varying ferrocene and xylene mixture solution flow rate between 0.25 and 0.30 mL/min, and changing the ferrocene concentration in xylene solution. Ferrocene concentration is 0.05 g/mL in this experiment. Temperature-time schedule of the synthesis process: both isothermal and non-isothermal conditions were used with maximum temperature of the reaction zone in the range of 800−900°C. After synthesis, the CNTs were cooled in inert gas (argon) flow (500 mL/min). The total experimental time varied from 3 h to 5 h with duration of actual growth stage 30−70 min. Two layers of vertically aligned CNT arrays are grown on a SiO_2 substrate without breaking through the vacuum, 40 min for the first layer, 70 min for the second, and the interval time is 30 min.

B. Characterization

The vertically aligned MWCNT arrays samples for SEM and Raman scattering analysis were as-prepared without further treatment. The as-synthesized samples were dispersed in ethanol with ultrasonic apparatus, and then were directly transferred to the copper grid for HRTEM measurements.

The product microstructures were investigated using SEM (JSM6490, Jeol), HRTEM (JEM3010, Jeol) and Raman Spectroscopy (HORIBA, T6400). In order to characterize the sample, HRTEM instruments were operated at the acceleration voltage of 200 kV, and for SEM instruments it was set as 20 kV. Diameter of the sample was measured directly from the HRTEM images, and the Raman scattering was also used to evaluate the tube diameters of single walled carbon nanotubes [15]. Raman spectra were recorded at room temperature with the excitation wavelengths of 532 nm.

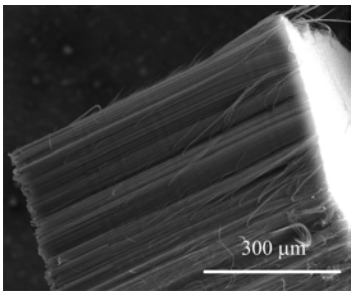

FIG. 1 SEM image of a sample vertically aligned MWCNT array.

III. RESULTS

A. Microstructures

Figure 1 shows the SEM image of one sample of the as-synthesized vertically aligned CNT arrays products. It can be seen that the length of tubes is typically more than 800 μm and the tubes are well aligned. Firstly, we investigated the purity of the vertically aligned MWCNT arrays and the diameter of the isolated SWCNTs of the as-synthesized samples from HRTEM analyses. Although the iron catalyst particles and tiny amorphous carbon were also observed in the samples, as shown in Fig.2 (a) and (b), the isolated SWCNTs were also observed (as shown in Fig.2(c)), as well as high amount of MWCNTs and very small amount of few-walled carbon nanotubes (as shown in Fig.2(d), typically <5 walls). Comprehensive analyses of SEM and HRTEM observations lead to the conclusion that the MWCNT products are composed of hollow tubes with average diameter ranging from 25 nm to 300 nm, the isolated SWCNTs have the diameter of about 1.3 nm.

B. Raman spectroscopy

Raman spectroscopy played an important role in analyzing the vibrational properties of CNTs [16, 17]. We also investigated the diameter of SWCNTs and the vibrational model of MWCNTs by the Raman spectroscopy using a 532 nm excitation laser.

Figure 3(a) shows the Raman spectrum taken from the surface of one synthesized sample. Figure 3(b) shows the spectrum from the scattering signals of the radial breathing mode (RBM) vibrations as shown in Fig.3(a). From this figure, we could easily determine the approximate tube diameter from the peak position of RBM by using a relation d=248/w, where d is the

DOI:10.1063/1674-0068/28/cjcp1502021

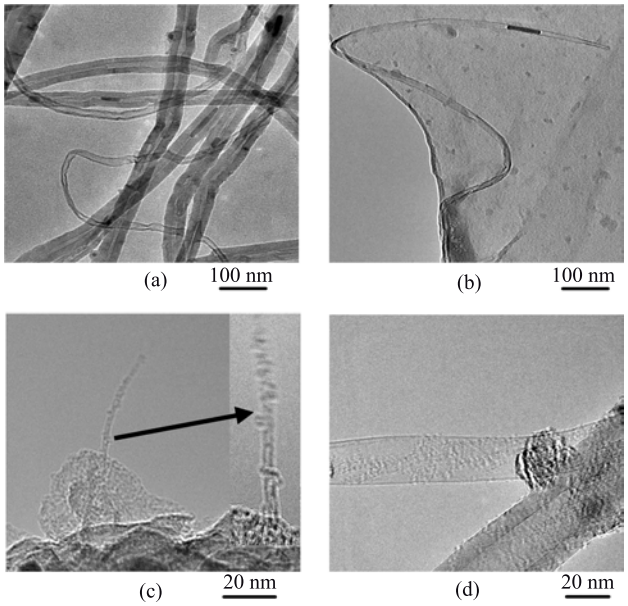

FIG. 2 (a) TEM image of MWCNTs. (b) HRTEM image of iron particle encapsulated in a CNT. (c) TEM image of an isolated SWCNT. (d) TEM image of some several-walled CNTs. Arrow

tube diameter and w is the peak position of the RBM [18, 19]. Therefore, the peaks of 130, 183, and 222 cm^{-1} are detected, corresponding to 1.9, 1.3, and 1.1 nm, respectively. From these peaks detected in the RBM region, we can conclude that the SWCNTs have diameter at about 1.3 nm, which agrees well with the results from HRTEM observations (Fig.2(c)). However, the Raman scattering peak intensity below 500 cm^{-1} is low, this probably means that the population of SWCNTs is rather low in the synthesized sample.

In the spectrum recorded for the tangential mode of vibration region (Fig.3(a)), we can see the intense Raman band at 1587 cm^{-1} that is assigned to the C−C stretching mode and is called G-band. Additional Raman bands at 1346 and 2698 cm^{-1} can also be seen in Fig.3(a), and they are called disorder induced band (1ω D-band and 2ω D-band). The scattering intensity is mostly related to the amount of amorphous carbon. Furthermore, from the Raman spectra taken from the middle wall and bottom surface of the vertically aligned MWCNT arrays, no signal of SWNTs RBM band is observed, which should be in the 100−500 cm^{-1} region if there are detectable SWCNTs (Fig.3 (b) and (c)). It is clear that no detectable amount of single walled carbon nanotubes existed in the middle side wall and bottom surface of the produced CNT arrays sample with FC method.

C. Base growth model validation

At present, there are two major growth mechanisms of carbon nanotubes: tip growth model and base growth

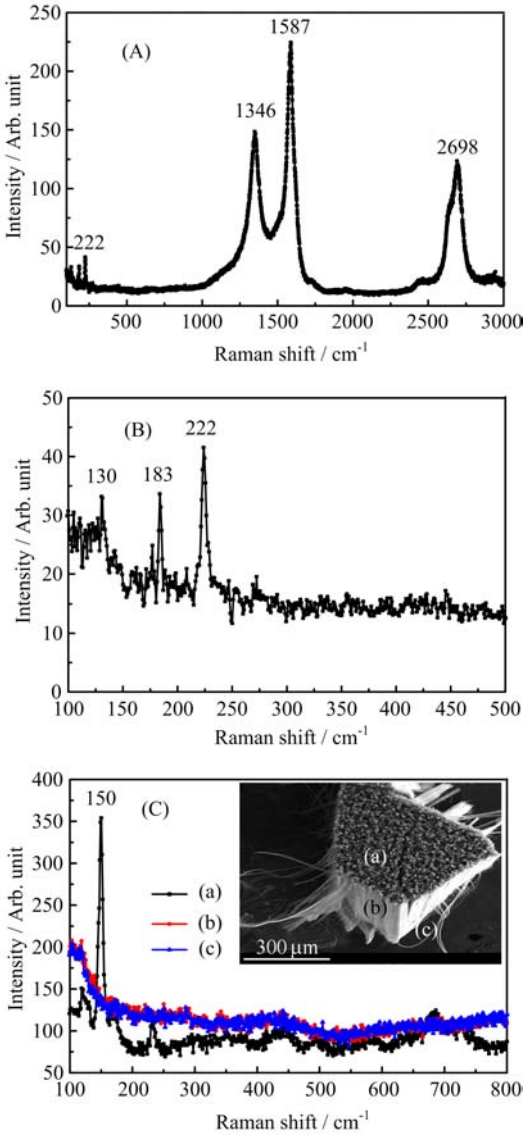

FIG. 3 Raman spectra of (A) the surface of one vertical aligned CNT sample and (B) enlarged view of the RBM region shown in (A). (C) Raman spectra of (a) the top surface, (b) middle wall, and (c) bottom surface of one vertical aligned CNT sample, and a SEM image of this sample is inserted.

model [20−23]. In order to check the growth mechanism of SWCNTs on top of the vertically aligned MWCNT arrays in this work, two layers of CNT arrays were grown on a SiO_2 substrate in two successive growth processes without breakdown of the vacuum. The thickness of each layer was precisely controlled by the growth time (see Fig.4(a)), the growth time was 30 min for the first layer and 70 min for the second.

In order to analyze the local structures and check the growth mechanism of the SWCNTs, the as-grown CNTs were investigated by SEM and Raman spectroscopy. Figure 4 (a) and (b) display typical low magnification SEM images and Raman spectra of one CNTs sample.

DOI:10.1063/1674-0068/28/cjcp1502021

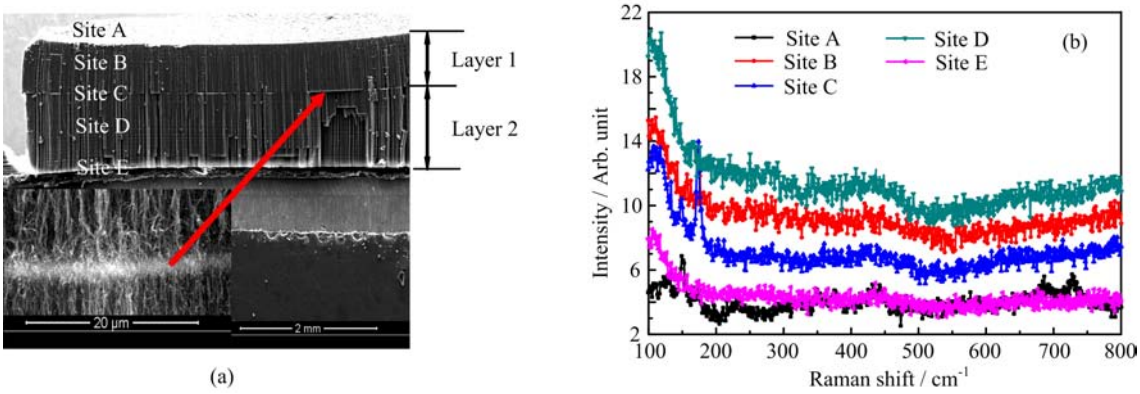

FIG. 4 (a) SEM image of a two-layer vertically aligned MWCNT array film sample, the insert at the left corner is the enlarged view of the interface between two nanotube array layers, and (b) Raman spectra taken at different sites (marked in (a)) in the same CNTs sample.

The results clearly revealed that the second layer grew at the bottom of the first layer, and the first layer was lifted up. The remarkable Raman spectra (as shown in Fig.4(b)) of as-grown CNTs in different sites (A, B, C, D, and E indicated in Fig.4(a)) proved there were also SWCNTs in the interface between two layers, as well as in the top surface of the first layer (as the arrow shows).

The results clearly showed that vapors of the carbon source and catalyst precursor (xylene and ferrocene) diffused through hundreds of microns of nanotube film and arrived at the bottom SiO_2 surface, even the substrate has been completely covered by the previously deposited first layer of nanotube arrays. The nucleation and growth of nanotubes catalyzed by Fe particles (from ferrocene) occured on the substrate surface, which acted as an active catalyst support. All of these results suggested that the vertically aligned CNT array samples were grown through the "base-growth" mechanism.

IV. DISCUSSION

Even though the synthesized samples generally consist of a mixture of metallic particles, vertically aligned MWCNTs, and isolated SWCNTs, the HRTEM and Ra-man spectroscopy analyses of the two-layer CNT array film samples indicate that, actually, both in the first layer and the second layer synthesis process, SWCNTs nucleate at and grow from the grown beginning on the substrate surface. The careful and systematic Raman spectra observations, shown in Fig.4(b), were also compared with Raman spectra taken at different sites of the sample. In all cases, it was found that the SWCNTs were only on the top surface of the vertically aligned MWCNT arrays, and the diameter of SWCNTs was about 1.3 nm. The SWCNTs had limited length (<400 nm) and existed on the top surface of each CNT array film layer, which was of particular interest since it can be observed both under HRTEM and Raman spectroscopy. It was clearly seen that SWCNTs were quite short and the RBM signals of SWCNTs were obvious.

On the basis of the observations described above, the scenario of the basic growth mechanism can be sketched in Fig.5. The first step (Fig.5(a)) of the growth process is the formation of a liquid nanoparticles of metal supersaturated with carbon. These nanoparticles originate from condensation of the metal plasma/vapor in the moderate temperature zone of the reactors. Upon cooling, the solubility limit of carbon decreases and carbon atoms segregate towards the surface where they precipitate. The second step (Fig.5(b)) is the formation of nanotube nuclei at the surface of the particle, which competes with the formation of a graphitic sheet wetting the surface of the particle (Fig.5(c)). Theoretically, both two transformation paths for carbon crystallizes exist. Indeed, their possibilities may be determined by some relevant factors, *e.g.*, the specific structures of nanoparticles of metal supersaturated with carbon and the cooling processes. Noticeably, for the second path (Fig.(c)/(e)), with augmenting the number of the layers of the graphene sheets wrapping the particle, the activity of the nanoparticles nuclei would decrease. This may differ in the first path, where the activity of the exposed nanoparticles nuclei to present CNTS may conserve. The third step (Fig.5(d)) is the nanotube growth which is likely to proceed by a progressive incorporation of carbon at the particle-nanotube interface [24]. Once expulsed, carbon crystallizes at the surface of the particle according to two competing transformation paths (Fig.5 (b) and (c)), which lead either to graphene sheets wrapping the particle and or to SWCNT nuclei with graphitic walls per-pendicular to the surface, which can been considered as a nonwetting process. When the nanotube nuclei are formed, growth should proceed through further incorporation of carbon. Carbon initially dissolved in the particle should continue to condense at the root of iron catalyst and SWCNTs became longer [25]. In order to achieve long nanotubes (Fig.5(d)), the growth should therefore continue for a sufficient long time. At the same time, iron

DOI:10.1063/1674-0068/28/cjcp1502021

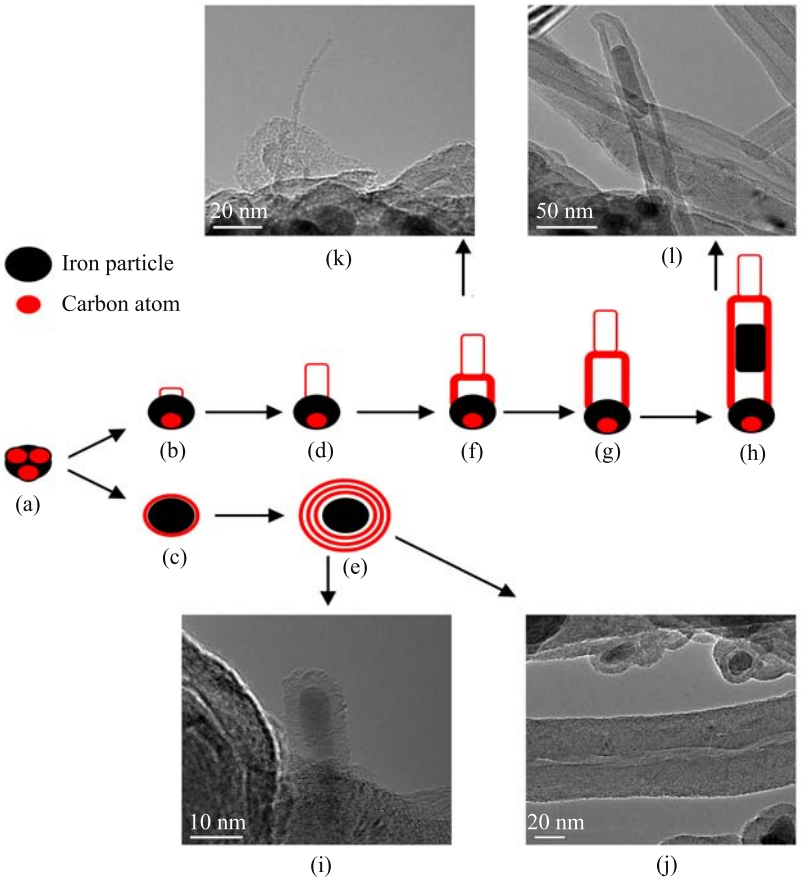

FIG. 5 The possible scenario of base growth mechanism. (a) Liquid iron particle containing carbon atoms. (b) Nucleation of SWCNTs emerging from iron nanoparticles when the particle size is much small. (c) Graphite sheet wrapping the particle. (d) SWCNTs elongate, and the diameter of tubes are related to the iron particle size. (e) Multilayer graphite sheets wrapping the particle. (f) Formation of MWCNTs nucleation when iron particles became larger. (g) Prolonging of MWCNTs. (h) An iron particle encapsulated in MWCNTs. (i)−(l) Some CNT morphologies under HRTEM, which can be seen as the evidences of the base growth mechanism.

catalyst and carbon atom source supplying, lead to the solidification and aggregation of the large nanoparticles, until the local temperature is too low. Indeed, one reasonable expectation is the temperature as an important factor in the growth mechanism: due to the temperature meaning the energy, the resulting thermodynamics motion of the nanotube nuclei at proper synthesis temperature may afford to lift up the former SWCNTs, and then yield the latter SWCNTs. Once the growth conditions have been perturbed in such a way, the growth has to be stopped. The remaining carbon, which was immediately available for the growth, can partly condense into amorphous carbon flakes embedding the particle (an example can be seen in Fig.5(j)), or condense into a few graphitic layers wrapping the particle (Fig.5(e)), thus build a buffer layer between the nanotubes and the particle (an example can be seen in Fig.5(i)).

The situation analyzed in Fig.5 (b), (d), (f), (g), and (h) defines another progress in which SWCNTs are observed to transform into MWCNTs where the walls are connected continuously to the layers wrapping the particle, through a complex process sketched in Fig.5 (d) to (h). The growth of MWCNTs from catalytic particles is a well-known process in chemical vapor deposition methods and can also be obtained from evaporation based routes [20, 26]. The present observations strongly suggest that, when assisted by a metallic catalyst, the formation of a MWCNT can also proceed from a dissolution-segregation process, that requires Fe catalytic particles, carbon segregation and diffusion intermediate become larger. The proof of the validity of the model is provided by the images shown in Fig.5 (k) and (l).

V. CONCLUSION

Vertically aligned MWCNT arrays with single or few-walled CNTs at top have been synthesized using FC method with xylene as carbon source, ferrocene as catalyst precursor in one pot. Through analyses with Raman spectroscopy and HRTEM, vertically aligned

DOI:10.1063/1674-0068/28/cjcp1502021

CNT arrays are characterized which are mainly comprised of well aligned MWCNT arrays, SWCNTs, and CNTs with few walls (typically <5 walls) on its top. Considering the "two steps bottom-up" growth of the two-layer CNT films experiments and the characterization results with HRTEM and Raman spectroscopy, the growth mechanism of SWCNTs and few-walled CNTs is believed to follow the base-growth mechanism: SWCNTs grow from their base at the very beginning growth when iron catalyst particles sizes are small. CNTs diameter becomes larger with iron catalyst particles size increasing, and vertical aligned MWCNT arrays will finally form.

VI. ACKNOWLEDGMENTS

This work was supported by the National Natural Science Foundation of China (No.11404302, No.11404304, and No.11204280) and the Open Project of State Key Laboratory Cultivation Base for Nonmetal Composites and Functional Materials (No.11zxfk19). We thank Dr. Jiang-feng Wang from CNRS/CEMES in France for his help in analysis of CNT Raman spectroscopy and Dr. Shuang-lin Hu from the Institute of Nuclear Physics and Chemistry CAEP for helpful suggestion.

[1] W. Z. Li, S. S. Xie, L. X. Qian, B. H. Chang, B. S. Zou, W. Y. Zhou, R. A. Zhao, and G. Wang, Science **274**, 1701 (1996).
[2] M. Zhang, S. Fang, A. Zakhidov, S. B. Lee, A. E. Aliev, C. D. Williams, K. R. Atkinson, and R. H. Baughman, Science **309**, 1215 (2005).
[3] J. Pan, C. Y. Chen, Y. L. Gao, and C. C. Zhu, Displays **30**, 114 (2009).
[4] B. Zhao, Z. L. Song, and J. H. Yang, Mater. Lett. **63**, 2556 (2009).
[5] L. Deng, M. Zhou, C. Liu, L. Liu, C. Y. Liu, and S. J. Dong, Talanta **81**, 444 (2010).
[6] U. Weissker, S. Hampel, A. Leonhardt, and B. Buchner, Materials **3**, 4387 (2010).
[7] J. Cheng, X. B. Zhang, F. Liu, J. P. Tu, H. M. Lu, Y. L. Sun, and F. Chen, Mater. Chem. Phys. **87**, 241 (2004).
[8] Y. Y. Fan, A. Kaufmann, A. Mukasyan, and A. Varma, Carbon **44**, 2160 (2006).
[9] X. Li, A. Cao, Y. J. Jung, R. Vajtai, and P. M. Ajayan, Nano Lett. **5**, 1997 (2005).
[10] M. Pinault, V. Pichot, H. Khodja, P. Launois, C. Reynaud, and M. Mayne-L'Hermite, Nano Lett. **5**, 2394 (2005).
[11] C. Singh, M. S. P. Shaffer, and A. H. Windle, Carbon **41**, 359 (2003).
[12] C. Singh, M. Shaffer, and K. Koziol, Chem. Phys. Lett. **372**, 860 (2003).
[13] A. Loiseau, J. Gavillet, F. Ducastelle, J. Thibault, O. Stephan, P. Bernier, and S. Thair, Comptes Rendus Physique **4**, 975 (2003).
[14] R. Bhowmick, B. M. Clemens, and B. A. Cruden, Carbon **46**, 907 (2008).
[15] A. M. Rao, E. Richter, S. Bandow, B. Chase, P. C. Eklund, K. A. Williams, S. Fang, K. R. Subbaswamy, M. Menon, A. Thess, R. E. Smalley, G. Dresselhaus, and M. S. Dresselhaus, Science **275**, 187 (1997).
[16] E. F. Antunes, A. O. Lobo, E. J. Corat, V. J. Trava-Airoldi, A. A. Martin, and C. Verssimo, Carbon **44**, 2202 (2006).
[17] Y. Murakami, S. Chiashi, E. Einarsson, and S. Maruyama, Phys. Rev. B **71**, 085403 (2005).
[18] M. S. Dresselhaus, G. Dresselhaus, A. Jorio, A. Filho, and R. Saito, Carbon **40**, 2043 (2002).
[19] H. Kuzmany, W. Plank, M. Hulman, Ch. Kramberger, A. Gruneis, T. Pichler, H. Peterlik, H. Kataura, and Y. Achiba, Eur. Phys. J. B **22**, 307 (2001).
[20] M. Kumar and Y. Ando, J. Nanosci. Nanotech. **10**, 3739 (2010).
[21] A. Gohier, C. P. Ewels, T. M. Minea, and M. A. Djouadi, Carbon **46**, 1331 (2008).
[22] H. Sugime, S. Esconjauregui, L. D'Arsié, J. Yang, T. Makaryan, and J. Robertson, ACS Appl. Mater. Interfaces **6**, 15440 (2014).
[23] H. Shahrokhabadi, M. Saeidi, M. Vaezzadeh, H. Shahivandi, and M. Salehian, J. Cryst. Growth **371**, 56 (2013).
[24] F. Ding, A. Rosen, and K. Bolton, Carbon **43**, 2215 (2005).
[25] E. F. Kukovitsky, S. G. Lvov, N. A. Sainov, V. A. Shustov, and L. A. Chernoza-tonskii, Chem. Phys. Lett. **355**, 497 (2002).
[26] D. Conroy, A. Moisala, S. Cardoso, A. Windle, and J. Davidson, Chem. Engin. Sci. **65**, 2965 (2010).

DOI:10.1063/1674-0068/28/cjcp1502021